Chemistry–A European Journal
Research Article
doi.org/10.1002/chem.202301845
Chemistry Europe
European Chemical Societies Publishing
www.chemeurj.org

Special Collection

Organotin(IV)-Decorated Graphene Quantum Dots as Dual Platform for Molecular Imaging and Treatment of Triple Negative Breast Cancer

I. Jénnifer Gómez,*[a, b] Karina Ovejero-Paredes,[c, d] José Manuel Méndez-Arriaga,[e] Naděžda Pizúrová,[f] Marco Filice,*[c, d] Lenka Zajíčková,[a, g] Sanjiv Prashar,[e] and Santiago Gómez-Ruiz*[e]

Dedicated to Professor Evamarie Hey-Hawkins, an inspiration for the new generation of inorganic chemists.

The pharmacological activity of organotin(IV) complexes in cancer therapy is well recognized but their large applicability is hampered by their poor water solubility. Hence, carbon dots, in particular nitrogen-doped graphene quantum dots (NGQDs), may be a promising alternative for the efficient delivery of organotin(IV) compounds as they have a substantial aqueous solubility, a good chemical stability, and non-toxicity as well as a bright photoluminescence that make them ideal for theranostic applications against cancer. Two different multifunctional nanosystems have been synthesized and fully characterized based on two fragments of organotin-based cytotoxic compounds and 4-formylbenzoic acid (FBA), covalently grafted onto the NGQDs surface. Subsequently, an *in vitro* determination of the therapeutic and theranostic potential of the achieved multifunctional systems was carried out. The results showed a high cytotoxic potential of the NGQDs-FBA-Sn materials against breast cancer cell line (MDA-MB-231) and a lower effect on a non-cancer cell line (kidney cells, HEK293T). Besides, thanks to their optical properties, the dots enabled their fluorescence molecular imaging in the cytoplasmatic region of the cells pointing towards a successful cellular uptake and a release of the metallodrug inside cancer cells (NGQDs-FBA-Sn).

Introduction

Cancer is one of the worldwide causes for death, which plays by its own rules, and many times does not respond the way it is supposed to. Finding the ideal treatment to cure this disease is one of the most tedious and sought after targets for researchers. In this field, metallodrugs have been successfully applied to treat numerous human diseases.[1,2] Research on the synthesis and applications of these metal complexes are currently bearing fruit in the field of biomedicine.[3] The best example resides in the well-known and effective cis-platinum drug.[4,5] Nowadays, studies with metallodrugs are shifting to the development of non-platinum metal-based agents to reduce the relatively high number of side effects associated with platinum treatments. Many organotin(IV) complexes have shown interesting *in vitro* and *in vivo* anticancer activity as new

[a] *Dr. I. J. Gómez, Assoc. Prof. L. Zajíčková*
Department of Condensed Matter Physics, Faculty of Science
Masaryk University
Kotlářská 2, 61137 Brno (Czech Republic)
E-mail: i.jennifer.gomez@udc.es

[b] *Dr. I. J. Gómez*
Centro Interdisciplinar de Química e Bioloxía (CICA)
Universidade da Coruña
Rúa as Carballeiras, 15071 A Coruña (Spain)

[c] *K. Ovejero-Paredes, Prof. Dr. M. Filice*
Nanobiotechnology for Life Sciences Group, Departamento de Química en Ciencias Farmacéuticas, Facultad de Farmacia
Universidad Complutense de Madrid (UCM)
Plaza Ramón y Cajal, 28040 Madrid (Spain)
E-mail: mfilice@ucm.es

[d] *K. Ovejero-Paredes, Prof. Dr. M. Filice*
Microscopy and Dynamic Imaging Unit
Fundación Centro Nacional de Investigaciones Cardiovasculares Carlos III (CNIC)
Calle Melchor Fernández Almagro 3, E-28029 Madrid (Spain)

[e] *Dr. J. M. Méndez-Arriaga, Prof. Dr. S. Prashar, Prof. Dr. S. Gómez-Ruiz*
COMET-NANO Group, Departamento de Biología y Geología, Física y Química Inorgánica, E.S.C.E.T.
Universidad Rey Juan Carlos
Calle Tulipán s/n, E-28933 Móstoles, Madrid (Spain)
E-mail: santiago.gomez@urjc.es

[f] *Dr. N. Pizúrová*
Institute of Physics of Materials, Czech Academy of Sciences
61662 Brno (Czech Republic)

[g] *Assoc. Prof. L. Zajíčková*
Central European Institute of Technology – CEITEC
Brno University of Technology
Purkyňova 123, 61200 Brno (Czech Republic)

Supporting information for this article is available on the WWW under https://doi.org/10.1002/chem.202301845

Special Collection *Part of a Special Collection on the p-block elements.*

chemotherapy agents in recent years.[6,7,8] Organotin(IV) carboxylates have been one of the most extensively studied classes of anticancer compounds since observing that they significantly reduce the growth of tumors when tested *in vivo*.[9] Likewise, triphenyltin(IV) and tricyclohexyltin(IV) derivatives have shown high cytotoxic activity against a variety of cell lines.[9,10,11] However, the possible application of the synthesized organotin derivatives was minimal due to their poor water solubility. Nevertheless, some modifications, such as difficult-to-control encapsulation or conjugation to liposomes,[12] and functionalization with specific organic molecules (*e.g.*, ditetrazine),[13] can enhance the applicability of the systems promoting better pharmacological performance and facilitating the administration of these potent anticancer organotin(IV) metallodrugs.[14]

Due to the problems mentioned above, the design and development of novel technologies based on nanostructured materials have grown exponentially.[15–17] Nanomaterials are an excellent choice in different areas of biomedicine,[18–22] but especially in drug-delivery and encapsulation due to their small sizes and large specific surface area. This usually increases the cellular uptake and reduces the degradation of the drugs, enhancing their potential to be used as diagnostic tools and to deliver the therapeutic agents to specifically targeted sites in a controlled manner.[23] For instance, nanoparticles created *via* ultrasonic irradiation containing organotin(IV) complexes have been prepared previously in two isolated studies.[24,25] However, it was not until recently when the strong therapeutic potential of organotin(IV) compounds loaded in nanostructured and mesoporous silica nanoparticles has been demonstrated by our group both *in vitro* and *in vivo*.[26–32]

In this regard, carbon dots (CDs) are an ideal nanomaterial to create a vehicle that can simultaneously enable bioimaging, disease detection, and drug delivery.[33] CDs are rising stars in the carbon family and nanomedicine, due to their excellent properties, such as biocompatibility, water solubility, low cytotoxicity, low-cost production and tunable fluorescence.[34–37] Overall, the combination of these unique properties, including small size and surface functionalization, makes CDs a superior choice for various applications compared to traditional carbon materials such as carbon nanotubes or graphene, specifically in biomedical applications. Engineering the CDs surface can enhance their biomedical applications.[38–40] Thus, for drug loading a covalent approach is usually more effective and controllable compared with supramolecular interactions,[41,42] since the covalent binding might significantly reduce drug leakage and subsequently minimize unwanted side effects.[43,44] In the context of CDs as drug supports, covalent drug-loading method remains almost unexplored. Therefore, in order to study a potential synergistic effect of the combination of CDs and organotin(IV) compounds in anticancer therapy, the preparation of nitrogen-graphene quantum dots and their subsequent drug loading was explored *via* covalent grafting with two different organotin(IV) metallodrugs containing two -SnR_3 moieties (R = Ph, cyclohexyl) which have been shown to play a critical role by promoting physicochemical changes of the materials and a modulation of the biological activities of the studied systems.

This study covers not only the preparation of multifunctional nanoplatforms based on amino-functionalized GQDs loaded with two different organotin(IV) compounds, but also the evaluation of the therapeutic potential of the synthesized systems against a triple negative breast cancer cell line (MDA-MB-231) *in vitro*. Furthermore, and considering the rich and bright photoluminescence of the NGQDs, the theranostic potential of the synthesized materials has also been explored observing that the systems are easily visible at different wavelengths in the confocal microscope, showing a clear internalization in cancer cell lines. Finally, a toxicity study of the systems was also carried out against a non-cancer cell line (kidney cells, HEK293T) to validate the therapeutic potential of the novel platforms.

Results and Discussion

Preparation and characterization of NGQD-FBA-Sn

We prepared a fluorescent and water-soluble NGQD-FBA-Sn metallodrug-delivery system by taking advantage of the high water solubility of NGQDs and the presence of amino groups that can be utilized for covalent functionalization.[41] Besides, the use of nitrogen-doped GQDs was preferred due to the superior optical properties offered by nitrogen doping. The advantages of forming a conjugate with enhanced aqueous solubility are the increase in biocompatibility and decrease in side effects and multi-drug resistance,[45] of the metal-based drug and which should result in an improvement in the activity *in vitro* against cancer cells.

The nitrogen-doped graphene quantum dots (NGQDs) were prepared following our previously reported simple and low-cost-effective bottom-up procedure, using a microwave reactor under controlled conditions (Figure 1 (*i*)).[46] Glucose and ethylenediamine have been used as carbon and nitrogen precursors. They display a quasi-spherical shape and various oxygen and nitrogen functional groups on the surface. Moreover, NGQDs exhibit excitation wavelength-dependent multicolor emission behavior (see further details in Supporting Information).[46]

Then, two different organotin(IV) carboxylates complexes containing different triphenyltin or tricyclohexyltin fragments were synthesized (further details SI, Figure S1–2), to study whether the incorporation of these compounds in NGQDs increases the cell uptake and selectivity towards cancer cells. The organometallic tin(IV) compounds were synthesized using the corresponding starting chlorides, namely, triphenyltin chloride and tricyclohexyltin chloride (Figure 1 (*ii*)) and the ligand 4-formylbenzoic acid (FBA) with an excess of Et_3N to form the corresponding tin carboxylate compounds FBA-Sn (for further details, see Supporting Information). Although the water solubility of these compounds is still poor, the derivatives bear a free aldehyde group that can react with the amino groups of the NGQDs dots to form an imino compound. FBA-Sn compounds were covalently attached to the NGQD surface *via* reaction with the amino groups (Figure 1 (*iii*)). The resulting hybrid systems were purified by size-exclusion chromatography

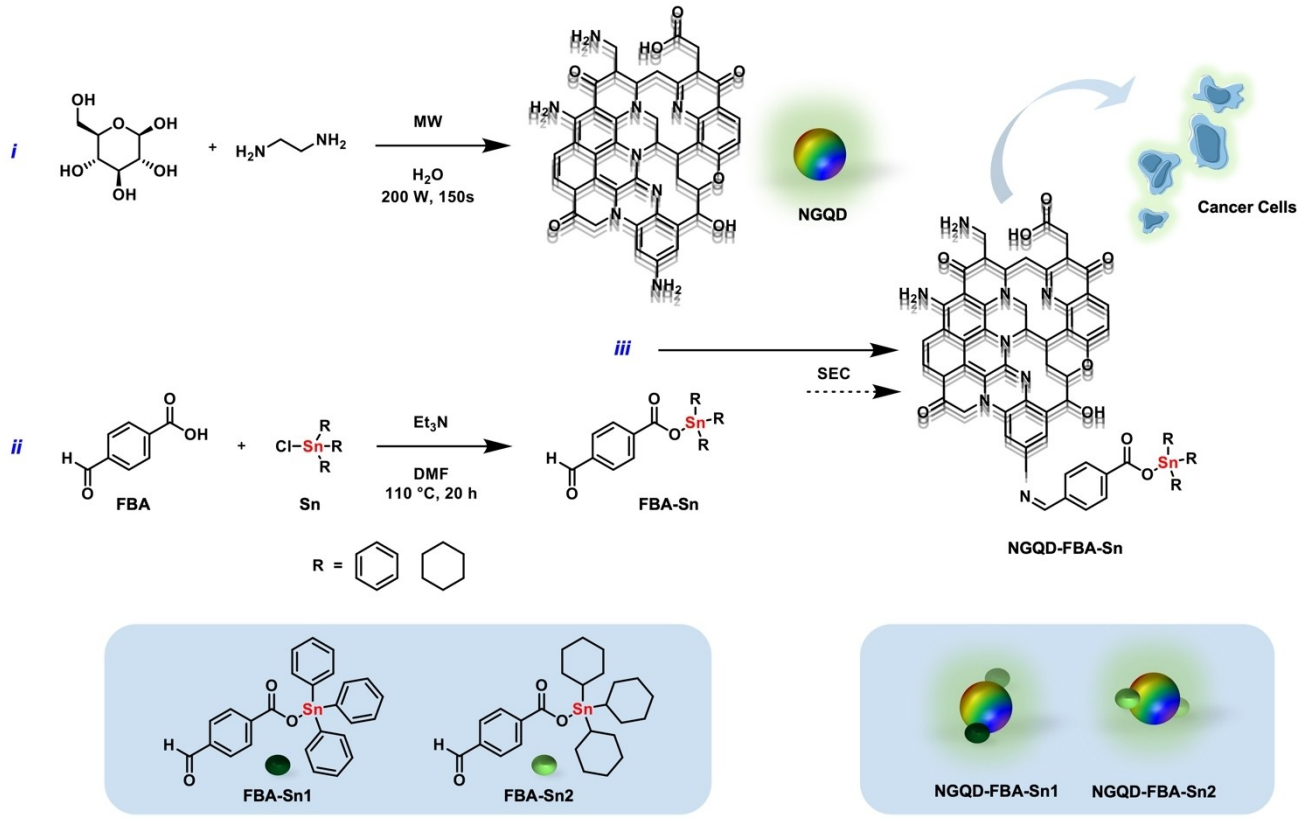

Figure 1. Representative scheme of the engineering NGQD-FBA-Sn drug delivery system. (*i*) Formation of the NGQDs *via* microwave (MW)-assisted hydrothermal method. (*ii*) Synthesis of the corresponding organotin(IV) compounds. (*iii*) Preparation and purification of the hybrids based on NGQDs and organotin(IV) compound *via* imine formation and SEC purification, (a hypothetical structure of the NGQD is depicted to clarify the imine-bond formation).

(SEC), during SEC the NGQD-FBA-Sn first fractions (*i.e.*, the largest) were collected to remove non-functionalized FBA-Sn and unmodified NGQDs.

Size and morphology of the prepared NGQD-FBA-Sn systems were analyzed by atomic force and transmission electron microscopy (AFM and TEM) and showed that the final nanoplatforms maintained a quasi-spherical morphology with sizes between ~4 and 8 nm (Figure 2a–c and Figure S3–5).

The chemical composition of NGQD-FBA-Sn1 was explored by scanning electron microscope-energy-dispersive X-ray spectroscopy (SEM-EDX). Notably, the presence of Sn was found along with the appearance of carbon, nitrogen and oxygen (Figure S6). Due to the high concentration on the SEM-EDX samples, and the low resolution of the SEM equipment, small nanoparticles could not be observed. Instead, agglomerates with the composition features of the hybrids were displayed in the graphs (Figure S6).

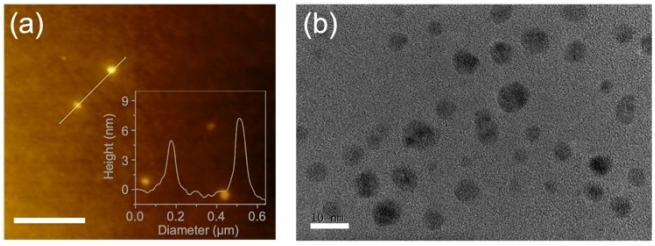

Figure 2. Morphology of NGQD-FBA-Sn1 system. (a) AFM image and (inset) corresponding height profile along the line, scale bar 500 nm. (c) TEM image, scale bar 10 nm.

The chemical structure of NGQD-FBA-Sn systems was characterized by ^{1}H NMR, Fourier transform infrared (FTIR) and X-ray photoelectron (XPS) spectroscopies. ^{1}H-NMR spectroscopic experiments supported the successful functionalization of the NGQD surface with FBA-Sn. The ^{1}H-NMR spectrum of NGQD-FBA-Sn showed the signals expected for the FBA-Sn complexes and the disappearance of the signal related to the aldehyde (~10 ppm), confirming the grafting onto the NGQDs surface through imine formation (Figure 3a and Figure S7). The FTIR spectrum of the NGQD-FBA-Sn revealed the characteristic signals of NGQDs and the FBA-Sn complex (Figure 3b). The Ar-H (751–689 cm^{-1}) band was observed for the FBA-Sn1 system and the C–H from the aliphatic region (2991–2790 cm^{-1}) for FBA-Sn2. A higher ratio of the signal intensities found for the C=N (1647 cm^{-1}) and N–H (1543 cm^{-1}) groups was observed for NGQD-FBA-Sn compared to that of NGQD, confirming that FBA-Sn, in all cases, was loaded on the surface of the dots via the imine bond.

The XPS analyses showed that pristine NGQDs contain carbon, nitrogen, and oxygen atoms,[46] whereas the composition of NGQD-FBA-Sn reflects a significant content of the Sn atom (Figures 3c, Figures S8–11 and Tables S1-S2). The XPS

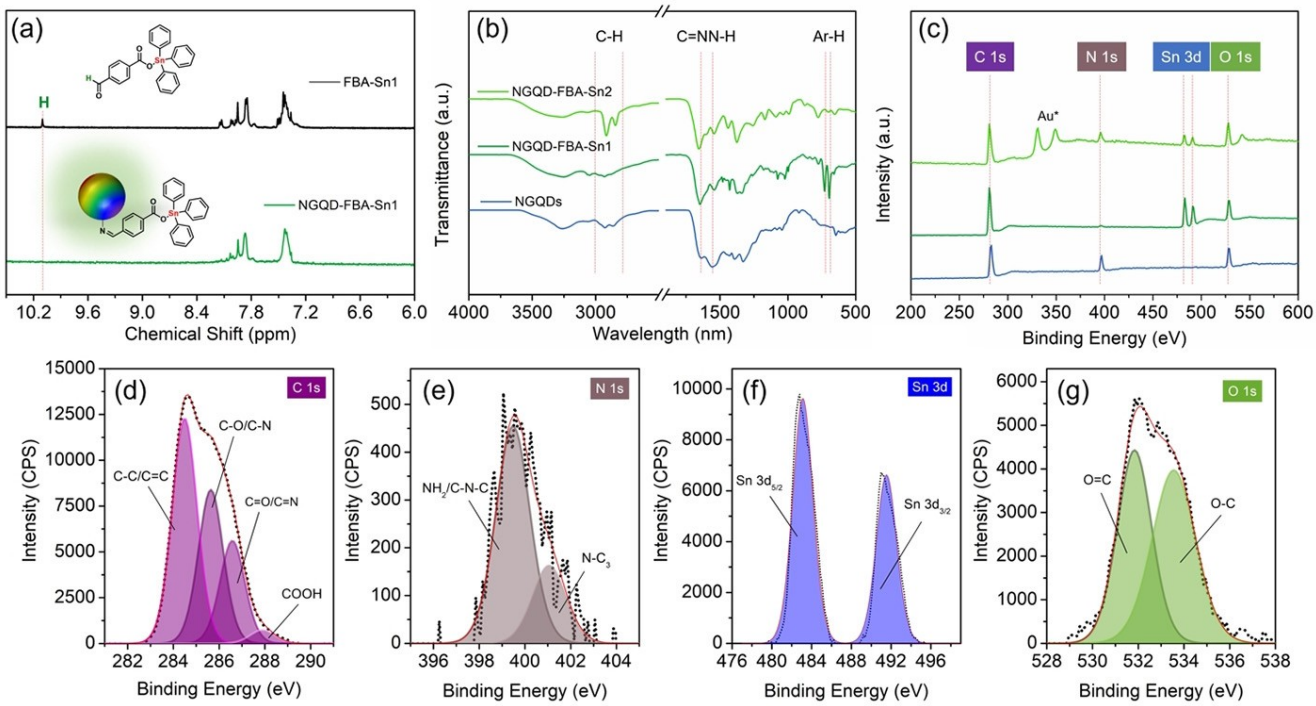

Figure 3. Chemical composition of NGQD-FBA-Sn: (a) ^{1}H NMR spectra of FBA-Sn1 and NGQD-FBA-Sn1 in DMSO-d_6. (b) FTIR spectra of pristine NGQDs and the corresponding NGQD-FBA-Sn hybrids. (c) XPS survey spectra, the colour code follows the pattern in (b). High-resolution XPS spectra of NGQD-FBA-Sn1 (d) C 1s, Au* from the substrate (e) N 1s, (f) Sn 3d and (g) O 1s.

elemental analyses agree with EDX results, confirming the successful attachment of FBA-Sn onto the surface of the dots. The chemical bonds for NGQD-FBA-Sn were analyzed by fitting high-resolution C 1s, N 1s, Sn 3d and O 1s XPS signals. C 1s was composed of four components corresponding to C–C/C=C (284.5 eV), C–O/C–N (285.64 eV), C=O/C=N (286.6 eV), and COOH bonds (287.9 eV) (Figure 3d and Figure S8 and Table S1–2). N 1s was deconvoluted into two components NH_2/C–N–C (399.5 eV) and N-C_3 (401.1 eV) (Figure 3e and Figure S9 and Table S1–2). The high-resolution Sn 3d peak displayed two components corresponding to Sn $3d_{5/2}$ and Sn $3d_{3/2}$ species (Figure 3f, Figure S10 and Table S1-2). The deconvolution of O 1s peak revealed two components O=C/Sn–O (531.9 eV), O–C (532 eV) and C–O–C (533.6 eV) bonds (Figure 3g, Figure S11 and Table S1–2). Notably, fitting the high-resolution nitrogen signal of pristine NGQDs resulted in 85.5 at.% of the N–H_2/C–N–C bonds.[46] For NGQD-FBA-Sn systems, it decreased to 73.6 at.% NGQDs-FBA-Sn1 and 79.4 at.% NGQDs-FBA-Sn2 (Figure 3e and Figure S9, and Tables S1–2). All these results verify the covalent hybrid formation through an aldehyde-to-amine crosslink and are in agreement with the conclusions taken from the interpretation of the FTIR spectra.

The absorption bands of NGQD-FBA-Sn systems in water were positioned at ~256–280 nm and ~372 nm, respectively (indicated by dashed lines in Figure 4). These bands exhibited slight shifts compared to those of NGQDs (Figure S12).[46] The shifts can be attributed to the presence of functional groups in the NGQD-FBA-Sn systems, causing changes in the π→π* (C=C) and n→π* (C=O and C=N) transitions.[46] The fluorescence

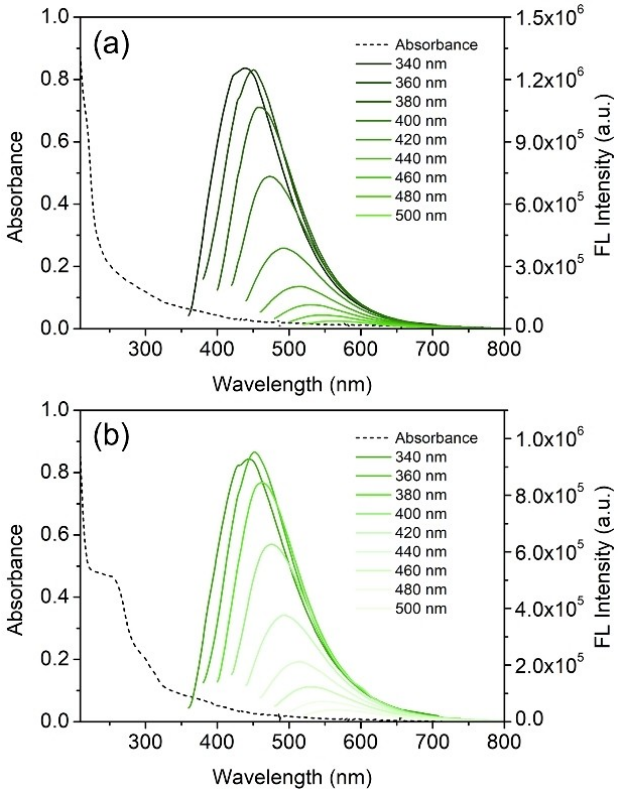

Figure 4. Optical properties of NGQD-FBA-Sn materials. Absorption (dash line) and emission spectra at different excitation wavelengths (color lines): (a) NGQD-FBA-Sn1 and (b) NGQD-FBA-Sn2. All spectra were measured in water at room temperature.

emission of NGQD-FBA-Sn exhibited the excitation-dependent behavior related to different radiative recombination pathways typical for the GQDs: band-to-band transitions, size effect, and other nitrogen and oxygen functional groups play a role in this multicolour emission (Figure 4).[46,47,48] A shift in the maximum excitation/emission wavelengths and a decrease in the fluorescence intensity from pristine NGQDs to the final nanosystem was also observed (Figure 4 and Table S3). Overall, the systems characterization techniques studied did not present significant differences between the systems NGQDs-FBa-Sn1 and NGQD-FBA-Sn2.

In vitro assessment of therapeutic potential of NGQD-FBA-Sn dual system

After the extensive physico-chemical characterization, the therapeutic potential of the synthesized materials was tested *in vitro* in human triple negative breast cancer cells (MDA-MB-231) and toxicity compared with kidney non-cancer cells (HEK293T) as possible target during elimination of NGQDs because of their ultrasmall size. The MTT viability assay was used for this purpose. As shown in Figure S13, tin-functionalized NGQDs show higher toxicity towards cancer cells than the unmodified NGQDs.

In order to easily compare the three studied materials, it is important to take into account that the non-functionalized NGQDs concentrations are shown in mg/mL while the concentrations of the tin-functionalized materials are in μM units (*i.e.*, Sn concentration), the equivalences between both are given in Table S4. For example, 1 μM of both NGQD-FBA-Sn1 and NGQD-FBA-Sn2 materials correspond to less than 1 mg/mL of NGQDs, therefore, it corresponds to 100% cellular viability of the non-functionalized material.

Effectively, with regards to the IC_{50} values (Table 1, the concentration of tin or material used to kill the 50% of the cells), tin-functionalized materials show more toxicity than the non-functionalized systems, and the viability of non-cancer cells (HEK293T) is higher than the viability of the breast cancer cells when using the same material concentration. These results suggest that the tin-functionalized systems (NGQD-FBA-Sn1 and NGQD-FBA-Sn2) present selectivity and are promising therapy agents for breast cancer management, as they also show an ample therapeutic range. Moreover, when comparing with other materials previously studied in our group, these new systems show better cytotoxic activity in cancer cells: IC_{50} for mesoporous silica (MSN-AP-FA-PEP-S-Sn) is around 3 μM while,[27] fibrous silica (FS-DT-FA-Sn), is 0.8 μM.29 These results suggest that these tin-derivative NGQDs are more efficient *in vitro* cytotoxic agents than the previously studied materials based on mesoporous silica nanoparticles or in fibrous silica nanomaterials.

Table 1. IC_{50} values of each material in both HEK293T and MDA-MB-231 cell lines.

Sample	HEK293T	MDA-MB-231
NGQDs	1.30 mg/mL	0.86 mg/mL
NGQD-FBA-Sn1	0.87 μM	0.41 μM
NGQD-FBA-Sn2	0.27 μM	0.10 μM

Assessment of potential of NGQD-FBA-Sn dual system to act as contrast agent for *in vitro* fluorescence imaging

After the toxicity evaluation, the *in vitro* fluorescence imaging enablement was addressed. Firstly, a thorough study of the fluorescence emission at different wavelengths was carried out using three different lasers (405, 488 and 561 nm) and collecting the emission between 430–480 nm, 500–550 nm and 590–650 nm, respectively (Figure 5). The goal of these experiments was to demonstrate that the synthesized materials showed emission at several wavelengths and therefore maintained the unique optical properties of the dots,[38,46,48] which is a very useful phenomenon, for example, for the follow up during *in vivo* assays.

As shown in Figure 5, both NGQDs are able to internalize inside of the triple negative breast cancer cells and both materials have fluorescence emission at all the studied wavelenghts, being a little bit higher when excited with the 488 nm excitation filter. With regards to the intracellular distribution, it seems that the NGQDs are located within the cytoplasm of the cells but not in the nuclei areas.

Conclusions

We have designed and synthesized nanoplatforms composed of the FBA-Sn complex loaded onto the surface of NGQDs through a covalent functionalization *via* imine group formation. The synthesized NGQD-FBA-Sn hybrids merge the carbon dots' optical properties with those of the FBA-Sn complex, bringing forward the possibility of their use as efficient metallodrugs in cancer therapy. In contrast with the pristine metal complex FBA-Sn, these tin-functionalized nanoparticles are dispersible in aqueous environments, which has opened up new pathways for the versatile metallodrugs preparation of theranostic dual systems based on bioimaging and drug-delivery systems. In this context, the cytotoxicity of the materials was studied in triple negative breast cancer and non-cancer human kidney cells (MDA-MB-231 and HEK293T, respectively), with promising results. In fact, the cell viability data showed that the nanoplatforms are more active when incubated with cancerous cells (MDA-MB-231) rather than when incubated with non-cancer cells (HEK293T). Regarding the bioimaging activity, upon incubation of the nanoparticles with MDA-MB-231 cells, fluorescence imaging can be promoted at different wavelengths, thus, suggesting the potential *in vivo* use of this kind of Sn-loaded NGQDs as polyvalent contrast agent in fluorescence imaging. Combining all these results, we can conclude that the synthesized materials are good candidates as theranostic agents. Nonetheless, ongoing studies, already in progress in our laboratories, are now focused on the potential *in vivo* applica-

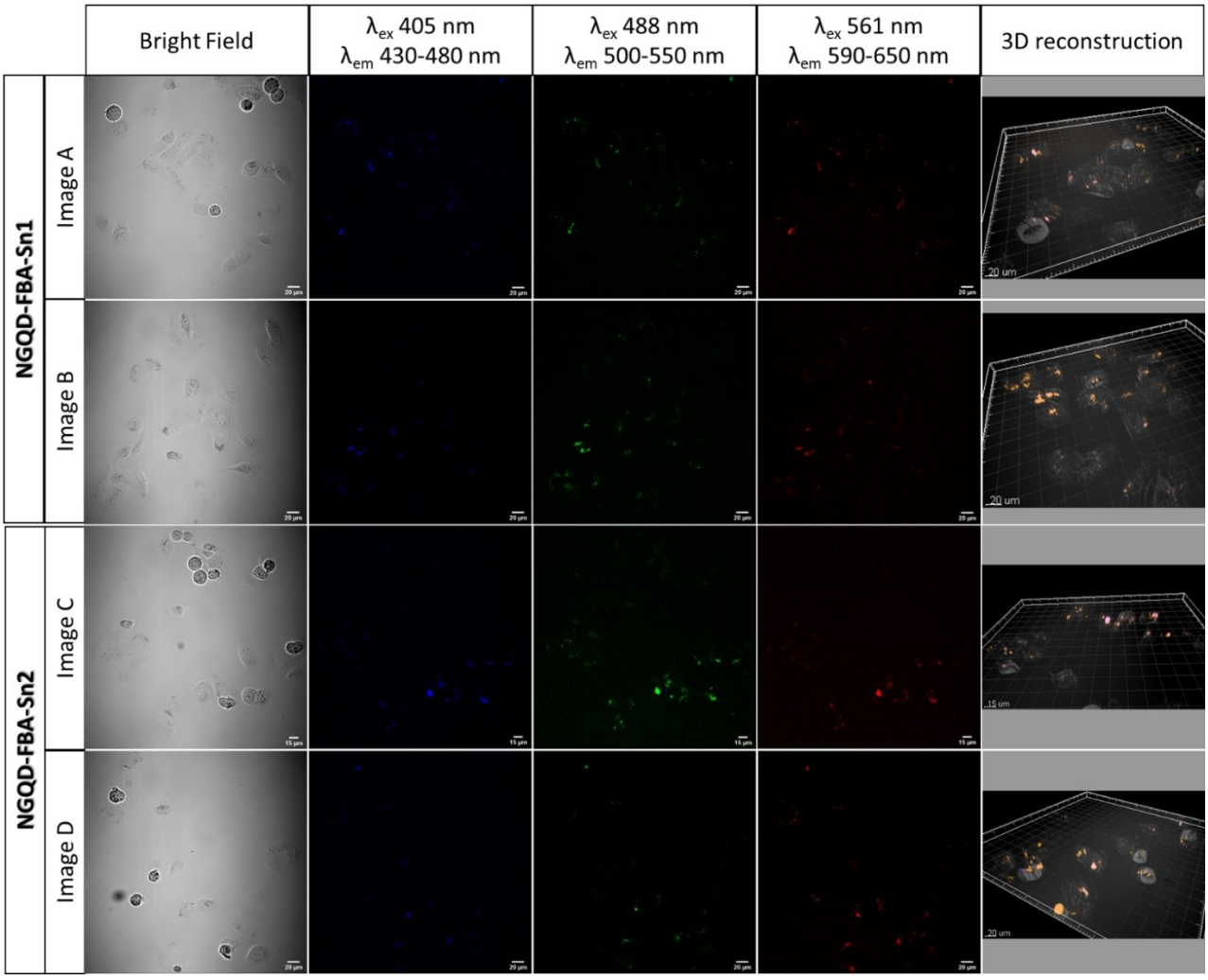

Figure 5. NGQDs-FBA-Sn1 and NGQDs-FBA-Sn2 confocal images of cellular internalization in MDA-MB-231 cells. Images series A and B correspond to NGQD-FBA-Sn1, while images series C and D show nanoparticles internalization in NGQD-FBA-Sn2. For images A, B, and D scale bar 20 μm, for image C scale bar 15 μm.

tion of this kind of materials using not only organotin-based metallodrugs but also other drugs of high clinical interest in different therapeutic approaches.

Experimental Section

Size and morphology

The size and morphology of NGQD-FBA-Sn were studied by atomic force microscopy (AFM). AFM images were obtained with a Dimension Icon (Bruker, Germany) in the tapping mode using an RTESPA-300 probe (300 kHz; 40 N/m) (Bruker, Germany). The AFM images were analyzed in Gwyddion 2.52.[49] The AFM samples were prepared by putting a diluted drop of the sample onto a freshly cleaved mica substrate. TEM images were taken with a JEM 2100F transmission electron microscope (JEOL, Japan) equipped with a Schottky cathode using a 200 kV electron beam. The TEM samples were prepared by putting a drop of sample solution on a commercially prepared Cu grid, coated with an amorphous carbon layer (Holey Carbon). Digital Micrograph and JEMS software were used for the analyses of the TEM images. SEM-EDX was carried out using Verios 460 L (Thermo Fisher, USA) 5 kV, to get elemental mapping composition. Before the measurement, the samples were mounted onto carbon tape.

Chemical composition

The chemical composition and structure of NGQD-FBA-Sn were evaluated by ^{1}H NMR, FTIR and XPS spectroscopies. ^{1}H spectra were obtained on 400 MHz Varian-Infinity Plus spectrometer (Bruker, Germany), using (DMSO-d_6) as a deuterated solvent. The ^{1}H NMR chemical shifts are reported in ppm relative to the tetramethylsilane signal (TMS, $\delta = 0.00$ ppm) using the residual solvent signal as an internal reference. The FTIR spectra were acquired with an Alpha FTIR spectrometer (Bruker, Germany), using a single diamond reflection attenuated total reflectance (ATR) accessory. Further details regarding the chemical composition are provided in SI. The XPS measurements were performed with an Axis Supra spectrometer (Kratos Analytical Ltd, UK). The quantitative atomic composition was determined from the survey XPS spectra taken at the pass energy of 80 eV. Lower pass energy of 20 eV was used to attain well-resolved XPS spectra of C 1s, N 1s, Sn 3d and O 1s for fitting

the chemical groups by the Casa XPS 2.3.17 software. The Shirley-type background was subtracted, and the fitting profiles were 30% Lorentzian and 70% Gaussian. Constrains of the full width at a half maximum (FWHM) and the peak positions were applied. The binding energy was calibrated by C–C/C=C groups at 284.5 eV. The XPS samples were prepared by putting a drop of aqueous solutions of the materials onto a silicon wafer sputtering with Au.

Optical properties

Optical properties of NGQD-FBA-Sn in water were investigated by UV-vis and fluorescence spectroscopies in standard 1-cm quartz cuvettes. UV-vis absorption spectra were recorded on a Cary 8454 UV-vis (Agilent Technologies, USA). Fluorescence spectra were measured on a F900 Fluorescent spectrometer (Edinburgh Instruments Ltd, UK). Rayleigh scattering and second diffraction order induced by the grating were removed by data processing.

In vitro experiments

Toxicity assay: The triple-negative human breast adenocarcinoma cell line MDA-MB-231 was cultured in DMEM-F12 supplemented with 10% FBS, 1% non-essential amino acids, 1% sodium pyruvate 100 mM and 1% penicillin/streptomycin. The culture was maintained at 37 °C in a humidified atmosphere with 5% CO_2. The human embryonic kidney (HEK293T) cells were maintained in a humidified atmosphere containing 5% CO_2 at 37 °C in Dulbecco's Modified Eagle's Medium (DMEM), supplemented with 1% penicillin/streptomycin, 1% sodium pyruvate, 1% glutamine, and 10% heat-inactivated fetal bovine serum (FBS). Both cell lines were subcultured every 2–3 days by treatment with TrypLE™ Express Enzyme (for MDA-MB-231) or trypsin (for HEK293T).

Total of 7.5×10^3 HEK293T or MDA-MB-231 cells were seeded in a 96-well culture plate and maintained at 37 °C and 5% CO_2. After 48 h, cells were incubated for 24 h with dispersions of each material (NGQDs, NGQDs-Sn1, NGQDs-Sn2) in culture medium without phenol red at different final Sn concentrations for the functionalized materials (0.1 μM, 0.5 μM, 1 μM, 5 μM, 25 μM, 100 μM, 250 μM and 500 μM) and final NGQDs concentrations for the non-functionalized material (0.1 mg/mL, 0.25 mg/mL, 0.5 mg/mL, 1 mg/mL, 2 mg/mL, 3 mg/mL, 4 mg/mL and 5 mg/mL). A positive control with the cells incubated with medium and a negative control incubating the cells with medium/DMSO 50/50 (v/v) were performed. After 24 h, the suspensions were removed and replaced by 100 μL of cell culture medium without phenol red and without serum. 10 μL of a 12 mM MTT (dimethylthiazolyl-diphenyl-tetrazolium bromide) solution (in cell culture medium without phenol red) was added to each well and mixed. After 3 h of incubation, the supernatants were removed with exception of 25 μL, and 100 μL DMSO were added to each well to dissolve the insoluble formazan salt, leaving it 15 min to react. Cell viability was estimated by measuring absorbance at 570 nm using a SPECTROstar Nano UV-vis plate reader (BMG Labtech).

Cellular uptake: 3×10^5 MDA-MB-231 cells (cultured as described previously) were seeded in a 6-well culture plate and incubated with the different modified materials (NGQDs-Sn1, NGQDs-Sn2) overnight, at a final material concentration of 1 μg/mL. Images were acquired with a Zeiss CLSM 780, 20x water objective at different wavelengths.

Acknowledgements

This work was supported by Operational Program Research, Development, and Education-Project 'MSCAfellow4@MUNI' (No. CZ.02.2.69/0.0/0.0/20_079/0017045) and the Spanish Ministry of Universities for a Maria Zambrano funding (RSU.UDC.MZ09) transferred by the European Union-Next Generation EU. We acknowledge CzechNanoLab Research Infrastructure (LM2018110), supported by the Ministry of Education, Youth and Sports of the Czech Republic (MEYS CR). We are grateful to Prof. Vladimír Šindelář and Prof. Petr Klan for allowing us to use the MW reactor, UV-vis and fluorescence spectrometer, supported by RECETOX research infrastructure (*via* MEYS CR under LM2018121). M.F. is grateful to Instituto de Salud Carlos III (ISCIII) for project No DTS20/00109 (AES20-ISCIII) and PI22/00789 (AES22-ISCIII). M.F. and K.O.P. acknowledge the support of Microscopy & Dynamic Imaging Unit of CNIC, Madrid, Spain. The Unit is part of the ReDiB-ICTS and has the support of FEDER, "Una manera de hacer Europa." The CNIC is supported by the Instituto de Salud Carlos III (ISCIII), the Ministerio de Ciencia e Innovación (MCIN) and the Pro CNIC Foundation, and is a Severo Ochoa Center of Excellence (grant CEX2020-001041-S funded by MICIN/AEI/10.13039/501100011033). We would also like to thank funding from the research project PID2022-136417NB-I00 financed by MCIN/AEI/10.13039/501100011033/ and "ERDF A way of making Europe", and from the Research Thematic Network RED2022-134091-T financed by MCIN/AEI/10.13039/501100011033.

Conflict of Interests

The authors declare no conflict of interest.

Data Availability Statement

The data that support the findings of this study are available in the supplementary material of this article.

Keywords: biomedical molecular imaging · graphene quantum dots · metallodrugs · organotin · theranostic

[1] P. Zhang, P. J. Sadler, *J. Organomet. Chem.* **2017**, *839*, 5.
[2] G. Gasser, I. Ott, N. Metzler-Nolte, *J. Med. Chem.* **2011**, *54*, 3.
[3] S. Gómez-Ruiz, G. N. Kaluderović, S. Prashar, E. Hey-Hawkins, A. Erić, Ž. Žižak, Z. D. Juranić, *J. Inorg. Biochem.* **2008**, *102*, 2087.
[4] N. Javadpour, *Urology* **1985**, *25*, 155.
[5] J. M. Williams, C. J. Whitehouse, *Br. Med. J.* **1979**, 10.
[6] Z. Liu, P. J. Sadler, *Acc. Chem. Res.* **2014**, *47*, 1174.
[7] Y. Ellahioui, S. Prashar, S. Gómez-Ruiz, *Inorganics* **2017**, *5*, 4.
[8] T. Anasamy, C. F. Chee, Y. F. Wong, C. H. Heh, L. V. Kiew, H. B. Lee, L. Y. Chung, *Appl. Organomet. Chem.* **2021**, *35*, e6089.
[9] C. Camacho-Camacho, I. Rojas-Oviedo, M. A. Paz-Sandoval, J. Cárdenas, A. Toscano, M. Gielen, L. B. Sosa, F. S. Bártez, I. Gracia-Mora, *Appl. Organomet. Chem.* **2008**, *22*, 171.
[10] M. Ashfaq, M. I. Khan, M. Kaleem Baloch, A. Malik, *J. Organomet. Chem.* **2004**, *689*, 238.

[11] L. Rocamora-Reverte, E. Carrasco-García, J. Ceballos-Torres, S. Prashar, G. N. Kaluderović, J. A. Ferragut, S. Gómez-Ruiz, *ChemMedChem* **2012**, *7*, 301.
[12] T. Boulikas, *Expert Opin. Invest. Drugs* **2009**, *18*, 1197.
[13] B. S. Murray, S. Crot, S. Siankevich, P. J. Dyson, *Inorg. Chem.* **2014**, *53*, 9315.
[14] W. A. Wani, S. Prashar, S. Shreaz, S. Gómez-Ruiz, *Coord. Chem. Rev.* **2016**, *312*, 67.
[15] A. B. Chinen, C. M. Guan, J. R. Ferrer, S. N. Barnaby, T. J. Merkel, C. a. Mirkin, *Chem. Rev.* **2015**, *115*, 10530.
[16] G. Hong, S. Diao, A. L. Antaris, H. Dai, *Chem. Rev.* **2015**, *115*, 10816.
[17] L. Wang, M. Marciello, M. Estévez-Gay, P. E. D. Soto Rodriguez, Y. Luengo Morato, J. Iglesias-Fernández, X. Huang, S. Osuna, M. Filice, S. Sánchez, *Angew. Chem. Int. Ed.* **2020**, *59*, 21080.
[18] L. L. Chamizo, Y. L. Morato, K. O. Paredes, R. C. Caceres, M. Filice, M. Marciello, *Polymers (Basel).* **2021**, *13*, DOI 10.3390/polym13223910.
[19] Y. L. Morato, K. O. Paredes, L. L. Chamizo, M. Marciello, M. Filice, *Polymers (Basel).* **2021**, *13*, DOI 10.3390/polym13172989.
[20] A. Lazaro-Carrillo, M. Filice, M. J. Guillén, R. Amaro, M. Viñambres, A. Tabero, K. O. Paredes, A. Villanueva, P. Calvo, M. del Puerto Morales, M. Marciello, *Mater. Sci. Eng. C* **2020**, *107*, 110262.
[21] A. Sánchez, K. Ovejero Paredes, J. Ruiz-Cabello, P. Martínez-Ruíz, J. M. Pingarrón, R. Villalonga, M. Filice, *ACS Appl. Mater. Interfaces* **2018**, *10*, 31032.
[22] M. Marciello, J. Pellico, I. Fernandez-Barahona, F. Herranz, J. Ruiz-Cabello, M. Filice, *Interface Focus* **2016**, *6*, 20160055.
[23] V. Weissig, T. K. Pettinger, N. Murdock, *Int. J. Nanomed.* **2014**, *9*, 4357.
[24] Z. Shariatinia, E. Asadi, V. Tavasolinasab, K. Gholivand, *Beilstein J. Nanotechnol.* **2013**, *4*, 94.
[25] Z. W. Li, X. H. Li, X. J. Tao, Z. J. Zhang, L. G. Yu, *Mater. Lett.* **2012**, *67*, 142.
[26] M. Z. Bulatović, D. Maksimović-Ivanić, C. Bensing, S. Gómez-Ruiz, D. Steinborn, H. Schmidt, M. Mojić, A. Korać, I. Golić, D. Pérez-Quintanilla, M. Momčilović, S. Mijatović, G. N. Kaluđerović, *Angew. Chem. Int. Ed.* **2014**, *53*, 5982.
[27] K. O. Paredes, D. Díaz-García, V. García-Almodóvar, L. L. Chamizo, M. Marciello, M. Díaz-Sánchez, S. Prashar, S. Gómez-Ruiz, M. Filice, *Cancers* **2020**, *12*, 187.
[28] D. Díaz-García, K. Montalbán-Hernández, I. Mena-Palomo, P. Achimas-Cadariu, A. Rodríguez-Diéguez, E. López-Collazo, S. Prashar, K. O. Paredes, M. Filice, E. Fischer-Fodor, S. Gómez-Ruiz, *Pharmaceutica* **2020**, *12*, 512.
[29] K. Ovejero-Paredes, D. Díaz-García, I. Mena-Palomo, M. Marciello, L. Lozano-Chamizo, Y. L. Morato, S. Prashar, S. Gómez-Ruiz, M. Filice, *Biomater. Adv.* **2022**, *137*, 212823.
[30] P. C. Choudante, S. K. Nethi, D. Díaz-García, S. Prashar, S. Misra, S. Gómez-Ruiz, C. R. Patra, *Biomater. Adv.* **2022**, *137*, 212819.
[31] D. Díaz-García, S. Prashar, S. Gómez-Ruiz, *Int. J. Mol. Sci.* **2023**, *24*, 2332.
[32] D. Díaz-García, L. Sommerova, A. Martisova, H. Skoupilova, S. Prashar, T. Vaculovic, V. Kanicky, I. del Hierro, R. Hrstka, S. Gómez-Ruiz, *Microporous Mesoporous Mater.* **2020**, *300*, 110154.
[33] C. Xia, S. Zhu, T. Feng, M. Yang, B. Yang, *Adv. Sci.* **2019**, *6*, 1901316.
[34] C. He, P. Xu, X. Zhang, W. Long, *Carbon* **2022**, *186*, 91.
[35] K. J. Mintz, M. Bartoli, M. Rovere, Y. Zhou, S. D. Hettiarachchi, S. Paudyal, J. Chen, J. B. Domena, P. Y. Liyanage, R. Sampson, D. Khadka, R. R. Pandey, S. Huang, C. C. Chusuei, A. Tagliaferro, R. M. Leblanc, *Carbon* **2021**, *173*, 433.
[36] S. Y. Lim, W. Shen, Z. Gao, *Chem. Soc. Rev.* **2015**, *44*, 362.
[37] R. Wang, K. Q. Lu, Z. R. Tang, Y. J. Xu, *J. Mater. Chem. A* **2017**, *5*, 3717.
[38] L. Đorđević, F. Arcudi, M. Cacioppo, M. Prato, *Nat. Nanotechnol.* **2022**, *17*, 112.
[39] X. Xu, Y. Li, G. Hu, L. Mo, M. Zheng, B. Lei, X. Zhang, C. Hu, J. Zhuang, Y. Liu, *J. Mater. Chem. C* **2020**, *8*, 16282.
[40] I. Jénnifer Gómez, M. Russo, O. A. Arcidiacono, E. M. Sánchez-Carnerero, P. Klán, L. Zajíčková, *Mater. Chem. Front.* **2022**, *6*, 1719.
[41] I. J. Gomez, B. Arnaiz, M. Cacioppo, F. Arcudi, M. Prato, *J. Mater. Chem. B* **2018**, *6*, 5540.
[42] S. Mangalath, P. S. Saneesh Babu, R. R. Nair, P. M. Manu, S. Krishna, S. A. Nair, J. Joseph, *ACS Appl. Nano Mater.* **2021**, *4*, 4162.
[43] Z. Wang, X. Hong, S. Zong, C. Tang, Y. Cui, Q. Zheng, *Sci. Rep.* **2015**, *5*, 1.
[44] F. Yan, Y. Jiang, X. Sun, Z. Bai, Y. Zhang, X. Zhou, *Microchim. Acta* **2018**, *185*, 424.
[45] M. Zaki, S. Hairat, E. S. Aazam, *RSC Adv.* **2019**, *9*, 3239.
[46] I. J. Gómez, M. Vázquez Sulleiro, A. Dolečková, N. Pizúrová, J. Medalová, R. Roy, D. Nečas, L. Zajíčková, *J. Phys. Chem. C* **2021**, *125*, 21044.
[47] I. J. Gómez, M. Vázquez Sulleiro, A. Dolečková, N. Pizúrová, J. Medalová, A. Bednařík, J. Preisler, D. Nečas, L. Zajíčková, *Mater. Chem. Front.* **2022**, *6*, 145.
[48] H. R. A. K. Al-Hetty, A. T. Jalil, J. H. Z. Al-Tamimi, H. G. Shakier, M. Kandeel, M. M. Saleh, M. Naderifar, *Inorg. Chem. Commun.* **2023**, *149*, 110433.
[49] D. Nečas, P. Klapetek, *Cent. Eur. J. Phys.* **2012**, *10*, 181.

Manuscript received: June 8, 2023
Accepted manuscript online: August 4, 2023
Version of record online: September 18, 2023